# Two-phase continuum theory for windblown sand

James T. Jenkins[1,*] and Alexandre Valance[2]
[1]*School of Civil and Environmental Engineering, Cornell University, Ithaca, New York 14853, USA*
[2]*Institut de Physique de Rennes, Université de Rennes 1, Campus Beaulieu, 35 042 Rennes Cedex, France*

(Received 29 August 2017; published 16 March 2018)

We outline the derivation of a two-phase continuum theory for grains, jumping above a bed of sand, while accelerated by a turbulent shearing flow, colliding with the bed, rebounding, and, perhaps, generating other grains. Relations between the shear and normal stresses and vertical derivatives of components of the average particle velocity are determined by averaging the dynamical equations for the particle trajectories. This provides the closure for the system of differential equations that govern the behavior of the wind and particles above the bed. Boundary conditions are obtained by averaging the results of experiments on rebound and ejection of particles from a particle bed. We solve the resulting system of equations subject to the derived boundary conditions for steady, uniform flows over both particle and rigid beds, and obtain unsteady, uniform solutions and steady, nonuniform solutions that provide information regarding saturation times and lengths, respectively.

DOI: 10.1103/PhysRevFluids.3.034305

## I. INTRODUCTION

When a turbulent wind blowing over a bed of sand becomes sufficiently strong, a grain may be lifted from the bed by a strong, localized turbulent eddy. The drag of the air then accelerates it and it collides with the bed with increased momentum. Impacting grains rebound and eject other grains that may also be accelerated by the wind until a sufficient number of grains are participating in the process to diminish the wind near the bed and create a steady balance in the exchanges of momentum between the grains and the wind and the grains and the bed. The result is a steady cloud of grains with diameters between 100 and 500 $\mu$m that jump (Latin: saltare) over the bed. This saltation and an associated creep of particles rolling and sliding along the bed are the primary modes of the initial sand movement [1–5]. Here, we ignore the creeping grains and sketch the development of a two-phase continuum theory for saltation that may be unsteady and/or nonuniform.

Most existing transport models for unsteady or nonuniform aeolian flows focus on the relaxation to equilibrium that results from a temporal or spatial change of the flow strength. The characteristic time or length scale necessary to recover the equilibrium regime of transport is often referred to as the saturation time or saturation length, respectively [6]. One important issue is to determine the key physical mechanisms that drive this process.

It has been suggested [7,8] that the acceleration of the transported particles due to fluid drag is the limiting relaxation mechanism, resulting in an inertial saturation length that scales linearly with the product of the fluid-to-particle density ratio and the particle diameter. However, this line of argument disregards other mechanisms, such as the entrainment of bed particles by the fluid drag and/or grain-bed collisions [6], and the feedback of the transport layer on the fluid velocity. Later, it was argued [9] that the negative feedback of the particles on the fluid flow is the limiting mechanism in the saturation process, also controlled by the inertial length. Measurements in wind-tunnel experiments [9] provide an estimation of the saturation length compatible with the inertial length.

*Corresponding author: jim.jenkins@cornell.edu

 

Pahtz *et al.* [10,11] have recently developed an analytical model based on a depth-averaged continuum approach that takes into account the previously neglected mechanisms. The results of the model indicate that the relaxation of the particle speed and the particle concentration occur at the same time scale and the two relaxation mechanisms interact. This is clearly different from that based on the inertial length, but shares some common features: First, it is also independent of the flow strength, because the equilibrium speed does not depend on the turbulent shear rate, and second, it provides a similar order magnitude of about 2000 particle diameters for aeolian sand. The common features prevent the making of a definite statement concerning the relevant mechanism involved in the relaxation process.

In this paper, we follow the template established in the continuum modeling of Sauermann *et al.* [6] that initiated the renewed interest in the physics of windblown sand and the creation and migration of sand dunes. They formulated a depth-averaged, two-dimensional phenomenological model to predict the evolution in space and time of the average particle density and velocity, driven by a turbulent shearing flow over a horizontal particle bed. The model contained parameters that in the absence of better information were evaluated in comparisons with experiments and numerical simulations. The model predicted the dependence of the saturation flux on the strength of the steady, uniform, turbulent shearing flow and the times and distances necessary to reach saturation after changes in the strength of the flow or conditions at the bed; these mechanisms included both the drag of the wind and the collisional flux of particles from the bed. The predictions were in good agreement with those measured in experiments and simulations. Here, we take advantage of progress made in characterizing the interactions of particles with the bed and in the development of local continuum relations for the particle shear and normal stress above the bed to phrase a more detailed continuum model. It involves a system of partial differential equations and boundary conditions for the values above the bed of particle concentration, particle velocity parallel and perpendicular to the bed, and wind velocity. In principle, averaging these equations through the depth of the flow would permit us to recover the simpler model of Sauermann *et al.* [6].

In what follows, we first indicate how measurements of particle collisions with a bed of like particles and simple averaging lead to conditions on the average exchange of particle mass and momentum at the surface of the bed. This extends calculations in Creyssels *et al.* [12] to finite particle fluxes. We then review how local relations between the components of particle stresses and the particle velocity derivatives may be obtained by averaging the equations that govern the trajectories of single particles at each height of the trajectory. Here, the calculation of the particle shear stress by Jenkins *et al.* [13] is reviewed and extended to include a normal component that is proportional to the vertical derivative of the vertical particle velocity. Finally, we use these relations, the expression for the particle pressure, and the usual mixing length model for the turbulent shear flow, modified by the drag of the particles, in the equations of balance for the mass, horizontal and vertical momentum of the particles, and horizontal momentum for the wind, and obtain numerical solutions to boundary-value problems for a variety of flows. The theory may be extended to incorporate turbulent suspension [13,14] and the particle shear stress and pressure associated with particle collisions above the bed [15,16].

In steady, uniform situations, we calculate profiles of particle concentration and particle and gas velocities for flows that interact with a particle bed over a range of wind strengths and flows that interact with a rigid bed for a single wind strength and a range of particle holdups. Then, we consider a uniform, unsteady situation, associated with a change in the strength of the wind over a particle bed, and determine the change in profiles with time. Next, we calculate the evolution with distance of steady profiles over a rigid bed and determine that some of these steady solutions are unstable. Finally, taking as an upstream boundary condition the profiles associated with the flow of maximum particle flux over a rigid bed at a given wind speed, we determine their evolution with distance over a particle bed.

The structure of the continuum theory differs from those derived in the past in two respects. It includes expressions for the particle shear and normal stresses [13], calculated from rough averages of the equations for a particle trajectory, and it employs boundary conditions at the bed [12], determined from averages of mass and momentum exchanges measured in experiments [17] and numerical simulations [18,19]. The theory is complementary to recent discrete numerical simulations

of saltation and creep [20–24] that have the capacity to describe both steady and unsteady states. Consequently, they also can address issues such as the times and distances necessary to equilibrate after a change in the strength of the wind or the nature of the bed [10,11,24], and have the capacity to test the modeling assumptions made in deriving the continuum theory. An understanding of the mechanisms that underlie the times and distances that link steady states is important to an understanding of the instability of a flat bed [8,22,25–27] and the possible evolution of a sand heap into a crescent dune with a slip face [8,25,27–32].

The mass density and viscosity of the wind are denoted by $\rho^f$ and $\mu^f$, respectively, and, in what follows, lengths are made dimensionless by the grain diameter $d$, velocities by $(gd)^{1/2}$, where $g$ is the gravitational acceleration, and stresses by $\rho^s gd$, where $\rho^s$ is the mass density of the material of the grains.

## II. BOUNDARY CONDITIONS

We first consider the interaction between grains of the flow and grains of a particle bed. We denote the velocity of a grain by $\boldsymbol{\xi}$, its magnitude by $\xi$, and its vertical component by $\xi_y$. Measurements of collisions of single grains with a bed of like grains [17] show that the averages of the speed and vertical velocity components after a collision are related to values before a collision by

$$\bar{\xi}' = e(\boldsymbol{\xi})\xi = (0.87 - 0.72\sin\theta)\xi \quad \text{and} \quad \bar{\xi}'_y = e_y(\boldsymbol{\xi})|\xi_y| = \left(\frac{0.30}{\sin\theta} - 0.15\right)|\xi_y|, \tag{1}$$

where the primes denote upward values, $e$ and $e_y$ are coefficients of restitution, and $\theta$ is the angle between the incoming velocity vector and the surface of the bed. The total number $N$ of particles leaving the bed is seen to be $1 + 13(1 - e^2)(\xi/40 - 1)$, if $\xi > 40$; 1, if $3.70 < \xi < 40$; and 0, if $\xi < \sqrt{2}\sin\theta = 3.70$. In the former, more exactly than Creyssels *et al.* [12], we employ the vertical component of the impact velocity, when defining the particles captured by the bed as those that rebound less than a diameter.

We introduce the simple velocity distribution function

$$f(\boldsymbol{\xi}) = \frac{n_0}{2\pi T}\exp\left[\frac{-(\xi_x - u_0)^2 - \xi_y^2}{2T}\right], \tag{2}$$

in which the $n$, $u$, and $T$ are, respectively, the dimensionless number density, average flow velocity, and mean square of the velocity fluctuations, the subscript 0 indicates a quantity evaluated at the bed, and $T$ is uniform through the flow. The dimensionless number density is related to the concentration $c$ by $n = 6c/\pi$. We use the distribution function and Eq. (1) to calculate fluxes of mass and momentum at the bed. It differs from that measured by Ho *et al.* [33] in that it ignores the creeping particles.

The flux of mass $\dot{m}$ from the bed is calculated in the Appendix,

$$\begin{aligned}\dot{m} &= \int_{\xi_y \leqslant 0} (N-1)\xi_y f(\boldsymbol{\xi}) d\boldsymbol{\xi} \\ &= c_0 \frac{13}{40}\frac{6}{\pi^2}\frac{T^{3/2}}{u_0}\Bigg[\Bigg(1 - (0.87)^2 + 6800\pi(0.87)(0.72)e^{-\frac{u_0^2}{2T}} - 2(0.72)^2\frac{T}{u_0^2}\Bigg) \\ &\quad \times \left\{\frac{u_0}{\sqrt{T}}e^{-\frac{(40-u_0)^2}{2T}} + \left(\frac{\pi}{2}\right)^{1/2}\left[1 - \frac{u_0(40-u_0)}{T}\right]\mathrm{erfc}\left(\frac{40-u_0}{\sqrt{2T}}\right)\right\} \\ &\quad + 0.64\left(\frac{\pi}{2}\right)^{1/2}(0.72)^2\frac{T}{u_0^2}\mathrm{erfc}\left(\frac{40-u_0}{\sqrt{2T}}\right)\Bigg].\end{aligned} \tag{3}$$

This expression improves upon an approximation in Creyssels *et al.* [12] that is limited to values of the slip velocity $u_0$ less than 40. The corresponding fluxes of momentum in the horizontal and

vertical directions are, respectively [12],

$$\dot{M}_x = -\frac{\pi}{6}\int_{\xi_y\leqslant 0}(\bar{\xi}'_x - \xi_x)\xi_y f(\boldsymbol{\xi})d\boldsymbol{\xi} = c_0 T\left(0.35 + 0.07\frac{u_0}{T^{1/2}} - 0.33\frac{T^{1/2}}{u_0}\right) \tag{4}$$

and

$$\dot{M}_y = -\frac{\pi}{6}\int_{\xi_y\leqslant 0}(\bar{\xi}'_y - \xi_y)\xi_y f(\boldsymbol{\xi})d\boldsymbol{\xi} = c_0 T\left[0.12\left(\frac{u_0}{T^{1/2}} + \frac{T^{1/2}}{u_0}\right) - 0.08\right] + \frac{c_0 T}{2}. \tag{5}$$

In unsteady flows above a particle bed, Eq. (3) provides a relation between the values at the bed of the averages of the vertical velocity $v_0$, the concentration $c_0$, and the particle velocity $u_0$. In such flows, we employ it either in its exact form or as a linearization about the steady value of the slip velocity $u_0^0$, $\dot{m} = v_0 c_0 = \beta(u_0 - u_0^0)$, where $\beta = 1.7\times 10^{-3}$. When the rate of vertical momentum transfer $\dot{M}_y$ is equated to the pressure at the bed $p_0 = c_0 T$, Eq. (5) determines the ratio $u_0^0/T^{1/2}$ to be 4.6. Then, Eq. (4) relates the shear stress at the bed to the pressure $\dot{M}_x = s_0 = 0.6 p_0$. In steady flows, the mass flux vanishes; then, Eq. (3) requires that $u_0^0 = 23.06$ and $T = 25.14$.

Numerical simulations of collisions of single grains with a bumpy, rigid bed [34] show that the averages of the speed and vertical velocity components after a collision are related to values before a collision by

$$\bar{\xi}' = e(\boldsymbol{\xi})\xi = (0.90 - 0.25\sin\theta)\xi \quad \text{and} \quad \bar{\xi}'_y = e_y(\boldsymbol{\xi})|\xi_y| = \frac{0.65}{\sin\theta}|\xi_y|. \tag{6}$$

In this case, the mass flux (3) is not relevant, while [12]

$$\dot{M}_x = c_0 T\left(0.13 + 0.04\frac{u_0}{T^{1/2}} + 0.36\frac{T^{1/2}}{u_0}\right) \tag{7}$$

and

$$\dot{M}_y = c_0 T\left[0.26\left(\frac{u_0}{T^{1/2}} + \frac{T^{1/2}}{u_0}\right)\right] + \frac{c_0 T}{2}. \tag{8}$$

With these, at $y = 0$, $u_0 = 4.6T^{1/2}$ and $s_0 = 0.53 c_0 T$. Here, for simplicity, we ignore the detailed difference between the coefficients of restitution, the momentum fluxes, and the particle shear stress at rigid and particle beds, and employ the values for a particle bed for both particle and rigid beds. Finally, in steady flows over a rigid bed, the particle, or slip, velocity is not specified, but is given as a part of the solution when the dimensionless measure of the total mass over a unit area of the bed, the particle holdup $M^*$, is given. This is done by introducing an additional differential equation for the partial holdup, $I(y) = \int_0^y c(\varsigma)d\varsigma$, with boundary conditions $I(0) = 0$ and $I(h) = M^*$.

## III. PARTICLE STRESS

We next consider the motion of grains above the bed and the transfers of momentum associated with their trajectories in a turbulent shearing flow, and review how manipulating these equations and averaging the result leads to continuum relations between components of the particle stress and derivatives of the components of the particle velocity across the flow [13].

When the vertical drag on a particle is neglected, the $x$ components of the equations of motion for the upward and downward parts of a particle trajectory may be written

$$\xi'_y\frac{d\xi'_x}{dy} = \frac{D}{\sigma}(U - \xi'_x) \quad \text{and} \quad \xi'_y\frac{d\xi_x}{dy} = -\frac{D}{\sigma}(U - \xi_x), \tag{9}$$

where $y$ is the upward vertical coordinate, $D$ is the dimensionless drag coefficient, $\sigma \equiv \rho^s/\rho^f$, and $U$ is the local average fluid velocity. When we multiply these by $c\xi'_y$, sum them, and average, we

obtain

$$\overline{c\xi_y'^2 \frac{d}{dy}(\xi_x' + \xi_x)} = c\overline{(D/\sigma)\xi_y'(\xi_x' - \xi_x)}. \tag{10}$$

In this, we make the identifications of the average particle velocity $2u \equiv \overline{(\xi'_x + \xi_x)}$, the average particle pressure $p \equiv c\overline{\xi_y'^2} = cT$, and the average particle shear stress $2s \equiv c\overline{\xi'_y(\xi'_x - \xi_x)}$, and assume that the averages of products are products of averages. The result is a relation between the particle shear stress and the derivative of the particle velocity that involves the particle pressure and the drag coefficient [13],

$$s = \frac{\sigma p}{\alpha D}\frac{du}{dy}. \tag{11}$$

A comparison with discrete numerical simulations [13] indicates that the coefficient $\alpha$ is about 20.

Repeating the argument for the $y$ components of the equations of motion of the upward and downward trajectories with vertical drag now incorporated results in a similar relation between the vertical derivative of the vertical velocity $v \equiv \overline{(\xi'_y + \xi_y)}/2$ and the vertical component of the normal stress $b \equiv -c\overline{\xi'_y(\xi'_y + \xi_y)}/2$, where the quantity in parentheses vanishes when the upward and downward velocities have equal magnitude.

These expressions for the shear and normal stress of the particles permit the phrasing of a continuum theory for unsteady, uniform flows or steady, inhomogeneous flows that interact with rigid or particle beds.

## IV. GOVERNING EQUATIONS

Here, we write down the continuum equations that govern unsteady, nonuniform flow. We then employ the MATLAB solver bvp4c to obtain steady, uniform solutions and the solver pdepe to obtain solutions for both uniform, unsteady flows and steady, developing flows. The uniform, unsteady solutions are associated with the evolution with time of a uniform flow to a change in the shear stress of the wind at a large distance above the bed, and the steady, developing solutions apply to the adjustment with horizontal coordinate $x$ of a flow at constant wind speed to a change from a rigid to a particle bed. The advantage in writing continuum equations is that these existing solvers can easily be implemented to generate numerical solutions, and other mechanisms of momentum transfer, such as turbulent suspension [13,14] and collisions above the bed [15], can be easily incorporated into the theory. Solutions of the resulting equations can then provide information regarding characteristic times or distances associated with each mechanism.

### A. Unsteady, nonuniform flows

The system of equations that governs an unsteady, uniform, turbulent shearing flow with height $h$ of sand grains in air subject to a dimensionless turbulent shear stress $S^*$ at the top of the flow is the balance of horizontal particle momentum,

$$c\frac{\partial u}{\partial t} + cu\frac{\partial u}{\partial x} + cv\frac{\partial u}{\partial y} = \frac{\partial s}{\partial y} + c\frac{D}{\sigma}(U - u), \tag{12}$$

where $s$ is given by Eq. (11) and

$$D \equiv 0.3[(U - u)^2 + v^2]^{1/2} + 18.3/\mathrm{Re}, \tag{13}$$

with $\mathrm{Re} \equiv d(gd)^{1/2}/(\mu^f/\rho^f)$, in which $g = 980\ \mathrm{cm/s^2}$ is the gravitational acceleration; the balance of vertical particle momentum,

$$c\frac{\partial v}{\partial t} + cu\frac{\partial v}{\partial x} + cv\frac{\partial v}{\partial y} = \frac{\partial}{\partial y}(-p + b) - c\frac{D}{\sigma}v - c, \tag{14}$$

where $b = \sigma p(\partial v/\partial y)/(\alpha D)$; the conservation of particle mass,

$$\frac{\partial c}{\partial t} + c\frac{\partial u}{\partial x} + u\frac{\partial c}{\partial x} + c\frac{\partial v}{\partial y} + v\frac{\partial c}{\partial y} = \varepsilon\frac{\partial}{\partial y}\left(\frac{\partial c}{\partial y} - \frac{c}{T}\right), \tag{15}$$

where the last term is included to facilitate the numerical solution with the solver pdepe that requires a flux term in each equation, here with $\varepsilon = 0.01$ a small parameter and an expression for the flux that vanishes in a steady, uniform flow; and the balance of horizontal fluid momentum,

$$\frac{\partial U}{\partial t} + U\frac{\partial U}{\partial x} = \sigma\frac{\partial S}{\partial y} - cD(U-u), \tag{16}$$

where, with the assumption that the bed is hydrodynamically rough, $S = (1/\sigma)[\kappa(y+y_0)(\partial U/\partial y)]^2$, in which $\kappa = 0.41$ and $y_0 = 1/30$ is the bed roughness. For a hydrodynamically smooth bed, not considered here, $S = (1/\sigma)[1/\mathrm{Re} + \ell^2(\partial U/\partial y)]\partial U/\partial y$, where, following van Driest [35], $\ell = \kappa y\{1 - \exp[-(\sqrt{\rho_f S^{0*}}y/\mu_f)^{1/2}/19]\}$.

Because the value of $T$ in these equations is to be a constant, equal to that at the bed, where it is related to the particle velocity, we employ the diffusion equation $\partial T/\partial t = \delta\partial^2 T/\partial y^2$, with $\delta$ a constant of order one, to propagate the value of $T$ at the bed into the interior. Because pdepe requires a finite interval, the height of the flow is taken to be 500 particle diameters. A definite flow height also facilitates comparisons between different flows over a rigid bed and the transition between flows over rigid and particle beds.

The boundary conditions employed in the MATLAB solver pdepe at $y = 0$ at a particle bed are $U = 0$, $s = 0.6cT$, $v = \beta(u - u^0)$, and $\partial c/\partial y = -c/T$, where $T = (u/4.6)^2$. At a rigid bed, there is no vertical velocity and the particle holdup or the value of some other parameter must be provided. The boundary conditions at $y = h$ are $s = 0$, $S = S^{*0} + S^{*\prime}$, $b = 0$, and $\partial c/\partial y = -c/T$, where here the prime denotes a perturbation from a steady solution and, again, the superscript 0 denotes a value in the steady flow.

### B. Steady, uniform flows

In steady, uniform flows, the vanishing of the mass flux at the bed determines that $u(0) = 23.06$ and, in the system (12), (14), (15), and (16), the vertical particle velocity and derivatives with respect to $t$ and $x$ vanish. Then, Eq. (12) is

$$\frac{ds}{dy} = -c\frac{D}{\sigma}(U-u); \tag{17}$$

the inversion of Eq. (11) serves to determine the particle velocity,

$$\frac{du}{dy} = \alpha D\frac{s}{p}, \tag{18}$$

where $\alpha = 20$; the particle mass balances reduces to

$$\frac{dc}{dy} = -\frac{c}{T}, \tag{19}$$

where $T = 25.14$; and the fluid velocity is determined by

$$\frac{dU}{dy} = \frac{[(S^* - s)\sigma]^{1/2}}{\kappa(y+y_0)}. \tag{20}$$

The MATLAB solver bvp4c is used to determine steady solutions, only some of which we later show to be stable. At $y = 0$, this solver employs the boundary conditions $u = 23.06$, $s = 0.6cT$, and $U = 0$ at a particle bed. The last two of these are given at a rigid bed and, while it is natural

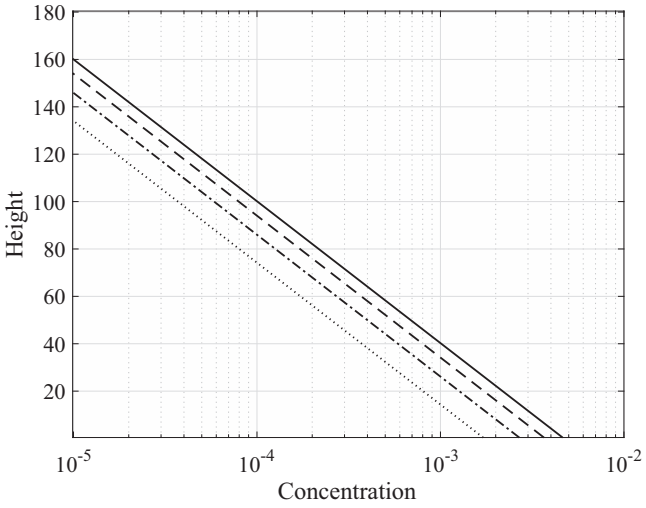


FIG. 1. Logarithm of the concentration vs dimensionless height for $d = 0.025$ cm. Spherical grains of sand in air at $S^* = 0.035$, 0.059, 0.065, and 0.080. Line weights increase with increasing values of $S^*$.

to specify the mass holdup at a rigid bed, we find it easier to obtain convergence by specifying the slip velocity and calculating the associated mass holdup. At $y = h$, we assume that $s = 0$. For both beds, the concentration at the bed is determined as part of the solution.

Because pdepe and bvp4c employ slightly different boundary conditions, a steady solution of bvp4c may differ slightly from the corresponding long-time stable solution of pdepe.

## V. NUMERICAL SOLUTIONS

### A. Steady, uniform flows

#### *1. Particle bed*

We first obtain a solution of the system of Eqs. (13)–(15) for a steady, uniform flow, in which $u = 23.06$, $T = 25.14$, and $s = 0.6\,cT$ at the bed, using the MATLAB solver bvp4c for two-point boundary-value problems. We take the distant shear stress $S^*$ to be 0.035, 0.050, 0.065, and 0.080, and consider sand particles with diameter $d = 0.025$ cm, specific mass in air $\sigma = 2200$, and kinematic viscosity $\mu^f/\rho^f = 0.15$ cm$^2$/s.

The parts of the predicted concentration profiles above a concentration of $10^{-5}$ are shown in Fig. 1. Jenkins *et al.* [13] indicate the relationship between these and those measured in experiments by Creyssels *et al.* [12]; the decay of the predicted concentration profiles is about half as fast as that measured in the experiments, but it can be increased to a value near that measured by incorporating suspension by the turbulent velocity fluctuations in the particle vertical momentum balance.

The predicted profiles of particle and gas velocity are shown in Fig. 2. Again, Jenkins *et al.* [13] indicate that these profiles are in good agreement with those measured by Creyssels *et al.* [12], and the agreement is improved by incorporating suspension by the turbulent velocity fluctuations.

We next test the profile of the stress predicted in such a steady, uniform situation against the results of a relatively simple numerical simulation [12]. The simulation employs particles ejected into a turbulent shearing flow with a Gaussian distribution of initial velocities and allows them to achieve a steady state through repeated interactions with the drag of the gas and collisions with the bed. The comparison is shown in Fig. 3. The agreement is good and offers additional support to the modeling in Sec. III that led to continuum expressions for the shear and normal stresses.

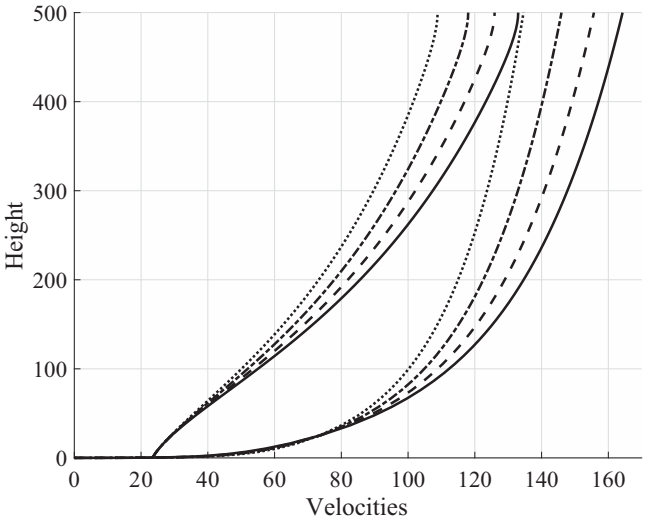


FIG. 2. Average dimensionless particle and gas velocities vs dimensionless height for $d = 0.025\,\text{cm}$. Spherical grains of sand in air at $S^* = 0.035$, 0.059, 0.065, and 0.080. Line weights increase with increasing values of $S^*$.

### *2. Rigid bed*

We now obtain solutions of the system of Eqs. (13)–(15) for a steady, uniform flow over a rigid bed. In this case, because the particle velocity at the bed is not specified, in addition to the distant shear stress, the total particle holdup, $M^* = \int_0^h c dy$, or the total particle flux, $Q = \int_0^h cu dy$, must be specified. However, we find it easier to obtain convergence if the problem is phrased in terms of the particle velocity at the bed—the slip velocity—rather than the flux or holdup. We take $S^* = 0.05$, consider a range of slip velocities, and use the one-to-one relationship between the slip velocity and

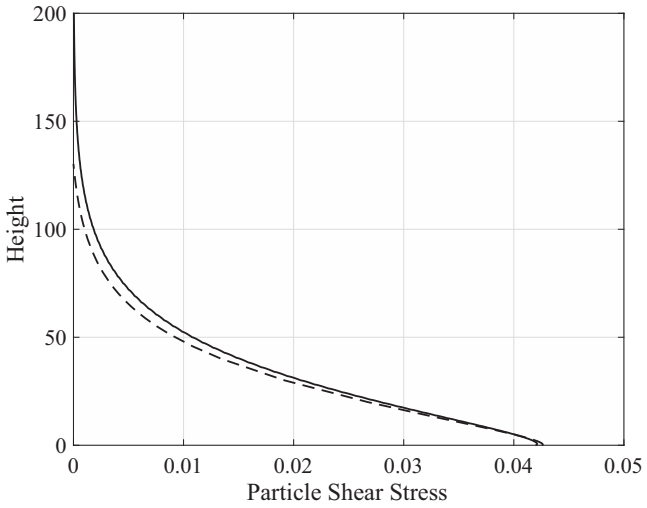


FIG. 3. Dimensionless continuum particle shear stress (dashed lines) and measured simulated particle shear stress (solid lines) vs dimensionless height for $d = 0.025\,\text{cm}$. Spherical grains of sand in air for $u_0 = 23.06$, $T = 25.14$, $S^* = 0.050$, and $\alpha = 20$.

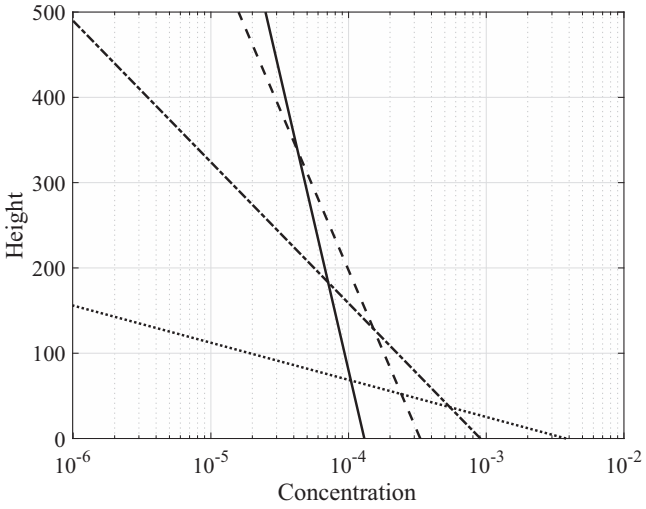


FIG. 4. Concentration vs dimensionless height for slip velocities of 15, 33, 48, and 60, with the line weights increasing with slip velocity. The corresponding values of the particle flux and holdup are 0.7 and 0.04, 1.8 and 0.04, 2.1 and 0.03, and 1.8 and 0.02, respectively.

the holdup to relate the two parametrizations. As before, we consider sand particles with diameter $d = 0.025\,\mathrm{cm}$. specific mass in air $\sigma = 2200$, and kinematic viscosity $\mu^f/\rho^f = 0.15\ \mathrm{cm}^2/\mathrm{s}$.

In Figs. 4 and 5 we show profiles of concentration and velocities for four values of the slip velocity. The height of the profiles increases with slip velocity, as the flow becomes less concentrated. The relationship between the total particle flux and the slip velocity is shown in Fig. 6, and Fig. 7 indicates the relationship between the particle flux and the holdup. Both the particle flux and the particle holdup are doubled valued over the range of slip velocity. Jenkins and Valance [34] and Berzi *et al.* [36]

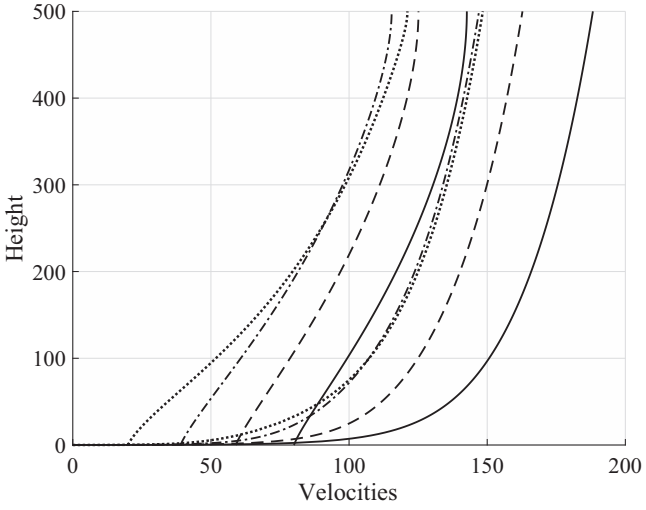


FIG. 5. Dimensionless particle and gas velocities vs dimensionless height for slip velocities of 20, 39, 59, and 80, with the line weights increasing with slip velocity. The corresponding values of the particle flux and holdup are 1.8 and 0.072, 3.5 and 0.065, 4.3 and 0.052, and 3.5 and 0.032, respectively.

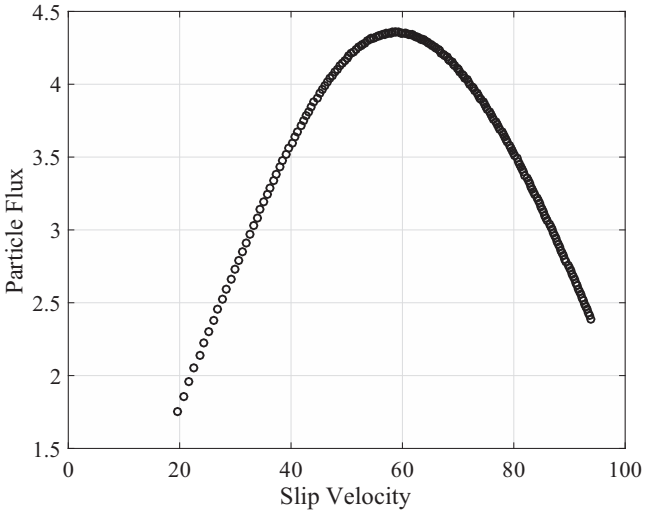


FIG. 6. The relationship between dimensionless particle flux and dimensionless particle slip velocity for $S^* = 0.05$.

obtained a similar but less complete relationship between the flux and holdup when considering periodic trajectories. They conjectured that the branch on which the flux decreases with increasing holdup is unstable. We will address this in a later section.

### B. Unsteady, uniform flow over a particle bed

We first use the unsteady solver to determine the evolution of the flow over a particle bed after a perturbation $S^{*\prime} = 0.0025$ to an initial, steady solution for which $S^* = 0.05$, $u_0^0 = 23.06$, and $h = 500$. The resulting profiles of particle concentration and the horizontal particle and gas velocities

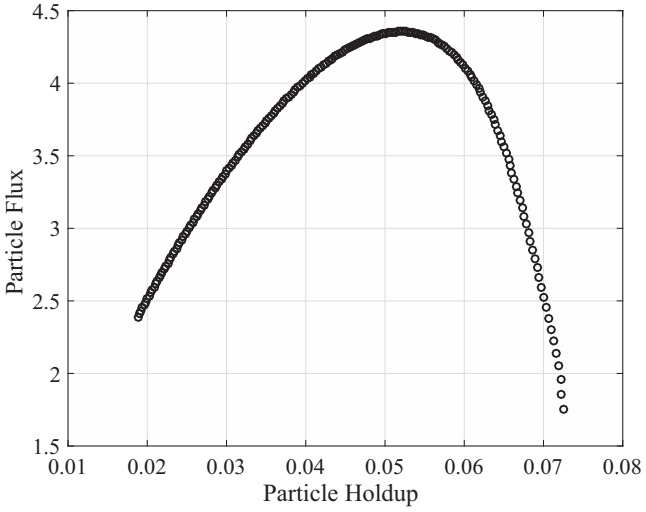


FIG. 7. The relationship between dimensionless particle flux and dimensionless particle holdup for $S^* = 0.05$.

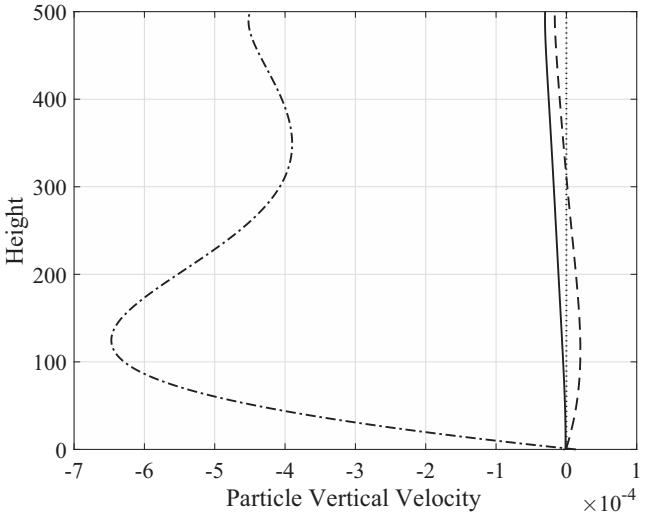


FIG. 8. Evolution of the dimensionless particle vertical velocity in space at three equal intervals between 0 and 12000 in units of dimensionless time with $\delta = 10$, for $d = 0.025$ cm. Spherical grains of sand in air at $S^{*\prime} = 0.0025, S^* = 0.05$, and $u_0^0 = 23.06$. Line weights increase with dimensionless time.

differ little from those at $S^* = 0.05$ and are not shown. The evolution of the profiles of vertical particle velocity and temperature are shown in Figs. 8 and 9.

The evolution of the profile of the particle vertical velocity is somewhat complicated, while, in contrast, that of the temperature, with the value of the parameter $\delta = 10$, remains relatively uniform as it varies in time.

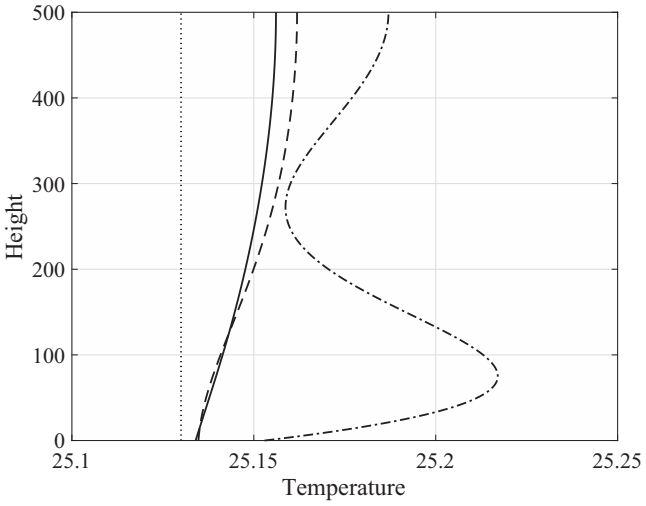


FIG. 9. Evolution of the dimensionless temperature in space at three equal intervals between 0 and 12000 in units of dimensionless time with $\delta = 10$, for $d = 0.025$ cm. Spherical grains of sand in air at $S^{*\prime} = 0.0025$, $S_0^* = 0.05$, and $u_0^0 = 23.06$. Line weights increase with dimensionless time.

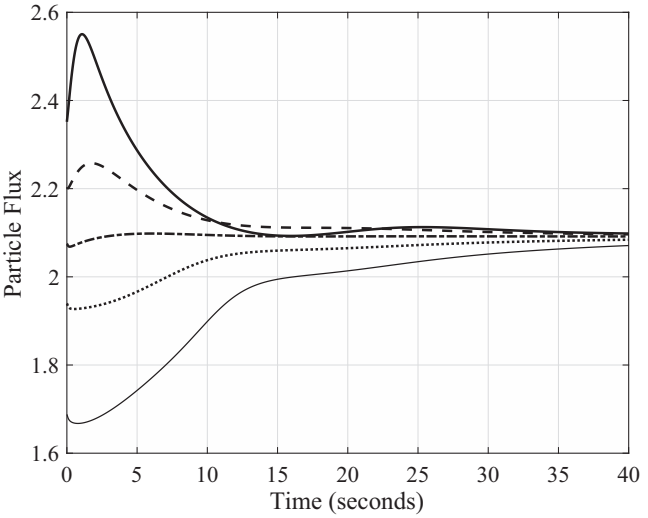


FIG. 10. Dimensionless particle flux vs time in seconds for spherical grains of sand in air showing the evolution with time on a particle bed for $S^* = 0.05$, from initial states that are steady states on a rigid bed with slip velocities of 19.0, 21.6, 23.1, 24.4, and 26.1, indicated by increasing line weights. Here, $d = 0.25$ mm, $\varepsilon = 0.01$, and $\delta = 5$.

If the unsteady versions of Eqs. (12) and (15) are combined and rearranged, an equation of evolution for the local particle flux $cu$ is obtained,

$$\frac{\partial}{\partial t}(cu) = -\frac{\partial}{\partial y}(vcu) + \frac{\partial s}{\partial y} + \frac{D}{\sigma}(cU - cu) + \varepsilon u\left(\frac{\partial c}{\partial y} - \frac{c}{T}\right). \tag{21}$$

If we average this equation through the depth of the flow and neglect the term proportional to $\varepsilon$, we obtain an expression for the total particle flux,

$$\frac{dQ}{dt} = v_0 c_0 u_0 - s_0 + \frac{1}{\sigma}\int_0^h D(cU - cu)dy, \tag{22}$$

where we have assumed that the product $vcu$ is negligible at the top of the flow. Assuming that the depth average of a product is the product of the depth averages and using the boundary condition on $v$, this may be written as

$$\frac{dQ}{dt} = \beta c_0 u_0\left(u_0 - u_0^0\right) - s_0 + \frac{\bar{D}}{\sigma}(h\overline{cU} - Q), \tag{23}$$

in which the overbars denote depth averages. Similarly, if the unsteady version of Eq. (15) for the concentration is averaged through the depth, we obtain an equation for the total particle holdup,

$$\frac{dM^*}{dt} = c_0 v_0. \tag{24}$$

Equations (23) and (24) correspond roughly to the two-equation continuum model of Sauermann *et al.* [6], which they express more simply by modeling some terms and closing others by comparison with experiment.

In Fig. 10, we show the variation of the total particle flux with time in the numerical solutions that evolve with time over a particle bed from different initial conditions. These show the particle fluxes evolving toward an equilibrium value from values below and above from initial conditions

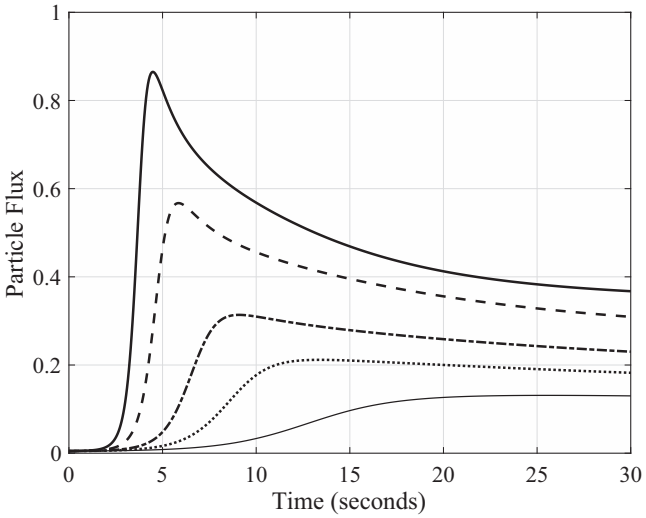


FIG. 11. Dimensionless particle flux vs time in seconds showing the evolution with time on a particle bed from a very small initial value ($Q = 0.005$ at $S^* = 0.009$) for increases in Shields numbers of 0.002, 0.003, 0.004, 0.006, and 0.008, indicated by increasing line weights. Here, $d = 0.25$ mm, with $\varepsilon = 0.01$ and $\delta = 1$.

that correspond to steady states over a rigid bed. The slip velocity of the steady state on the particle bed at $S^* = 0.05$ is $u_0 = 23$, so for $d = 0.025$ cm, 10 s roughly corresponds to 11.5 m. Bagnold (Fig. 6 in Ref. [1]) shows that uniform flow is attained in about 7 m, and when the initial particle flux is much smaller than the equilibrium particle flux, there is no overshoot; Andreotti *et al.* (Fig. 1 in Ref. [9]) see similar behavior over a shorter distance.

In Fig. 11, we show the evolution with time from an initial condition that corresponds to a steady state with a very small flux on a particle bed with increases in Shields number from 0.002 to

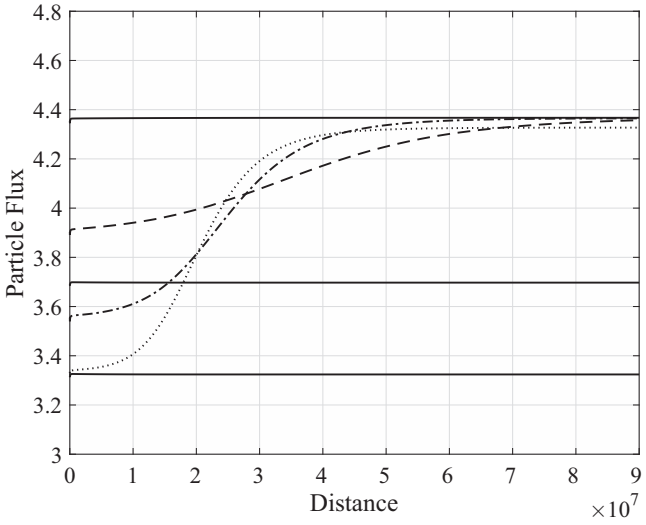


FIG. 12. Evolution of dimensionless total particle flux with distance over a rigid base for $S^* = 0.05$. The slip velocities of the three stable solutions (solid) are 59, 78, and 83, while those of the unstable solution are 37 (dotted), 40 (dotted dashed), and 45 (dashed).

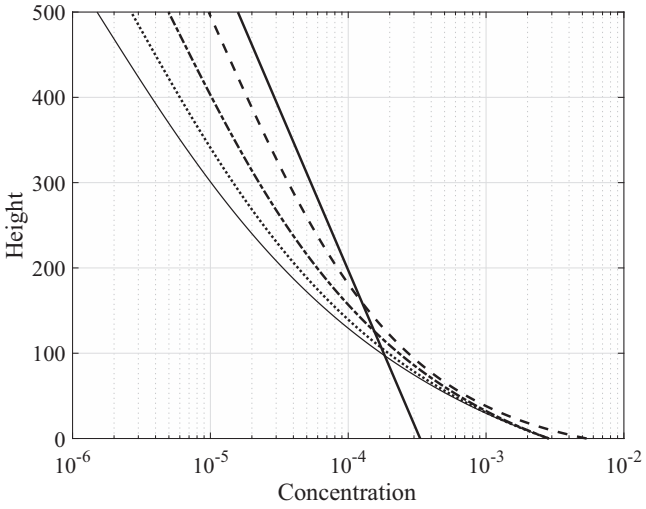


FIG. 13. Concentration vs height for four equal intervals of dimensionless distance between 0 and $10^6$, with $S^* = 0.05, u_0 = 59$, and $\delta = 5$. Line weights increase with distance.

0.008, corresponding to a range of friction velocities from 0.22 to 0.30 m/s. This figure reproduces both the overshoot and monotone approaches to equilibrium seen in experiments and simulations (e.g., Ref. [36]). The simple two-equation model of Sauermann *et al.* [6] also has the capacity to reproduce the relaxation seen in Figs. 10 and 11, and Fig. 11 is similar their Fig. 3 generated using the two-equation model; however, our results exhibit a slightly larger relaxation time. While we believe that the variation of $Q$ seen in experiments can be described as the behavior of a damped oscillator and, consequently, a linear two-equation model, we have not been able to write the right-hand sides of Eqs. (23) and (24) solely in terms of $Q$ and $M^*$. That is, we have not yet been successful at deriving a two-equation model from the system of Eqs. (12)–(16).

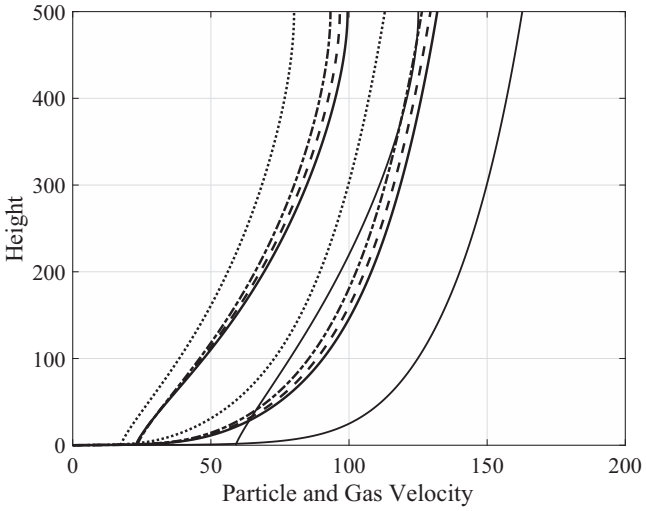


FIG. 14. Horizontal velocities vs height for four equal intervals of dimensionless distance between 0 and $10^6$, with $S^* = 0.05, u_0 = 59$, and $\delta = 5$. Line weights increase with distance.

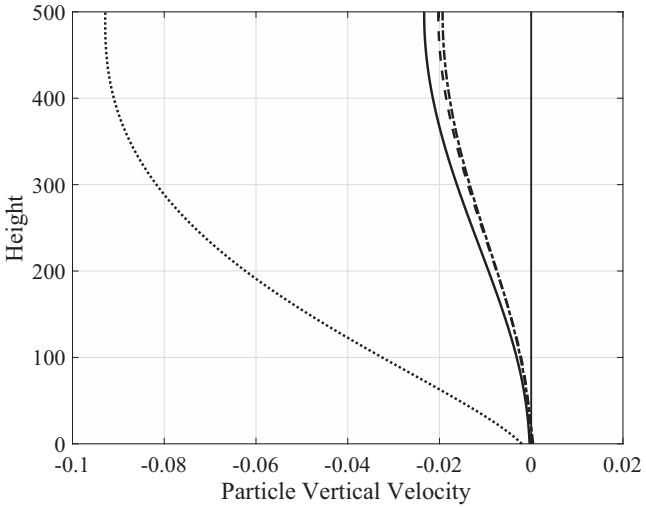


FIG. 15. Vertical velocity vs height for four equal intervals of dimensionless distance between 0 and $10^6$, with $S^* = 0.05, u_0 = 59$, and $\delta = 5$. Line weights increase with distance.

### C. Steady, nonuniform flow over a rigid bed

We next use the MATLAB solver pdepe on the nonuniform version of the system of Eqs. (9)–(12) over a rigid bed to test the stability of steady solutions by using them as initial conditions. In earlier work [34,37], we anticipated that solutions over a rigid bed for which the particle flux decreased as the particle holdup increased were unstable. We test this by determining whether a steady uniform solution will change when allowed to move along the rigid bed. This change can occur because of the presence of the terms on the left-hand side of the system, and an unstable solution and its particle flux can evolve with distance into that of a stable solution.

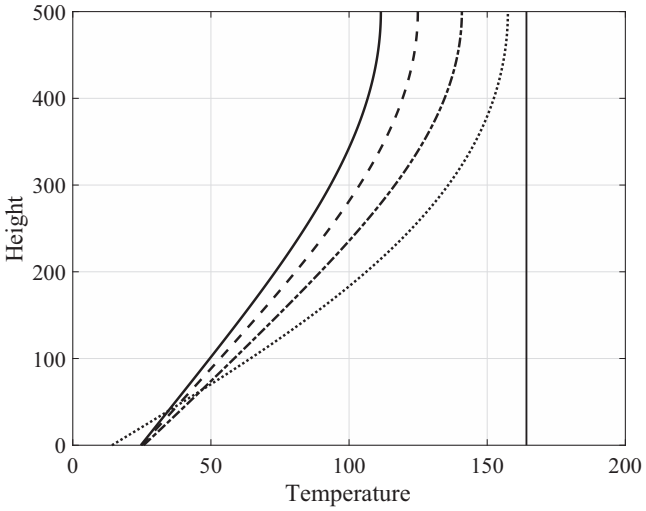


FIG. 16. Granular temperature vs height for four equal intervals of dimensionless distance between 0 and $10^6$, with $S^* = 0.05, u_0 = 59$, and $\delta = 5$. Line weights increase with distance.

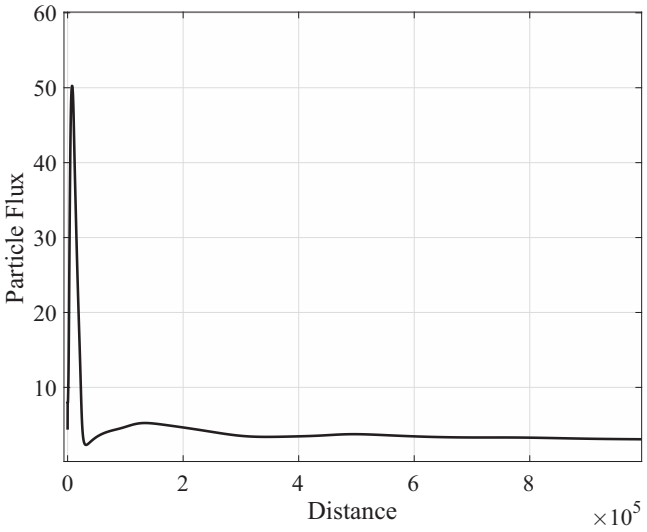


FIG. 17. Total particle flux vs dimensionless downstream distance, with $S^* = 0.05, u_0 = 59$, and $\delta = 5$.

In Fig. 12, we show the persistence of the particle flux of a stable solution and the migration of the particle flux from an unstable, steady solution to that of the steady, stable solution with the maximum particle flux.

Finally, we consider the steady, nonuniform situation in which a steady, uniform flow over an upstream rigid bed encounters and flows over a particle bed, adjusting with distance along the particle bed to the new conditions. We solve the nonuniform form of Eqs. (9)–(12) for a Shields parameter of 0.05, using the steady solution over the rigid bed with the maximum particle flux for $u_0 = 47$. This is the stable solution over the rigid bed that involves the largest particle flux.

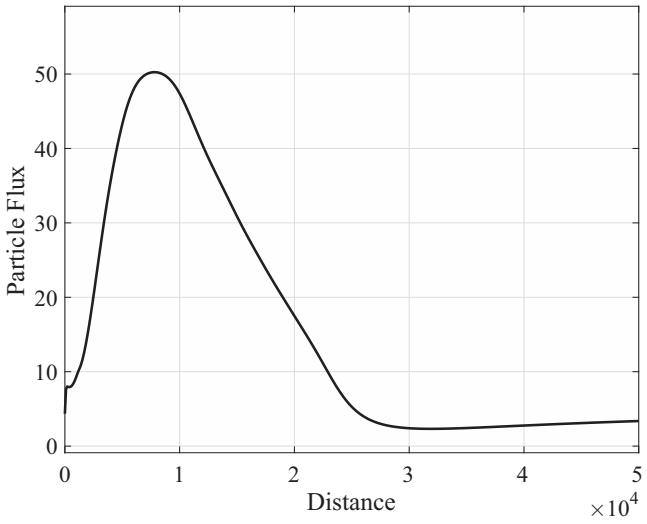


FIG. 18. Initial variation of the total particle flux vs dimensionless downstream distance, with $S^* = 0.05, u_0 = 59$, and $\delta = 5$.

Figure 13 shows the significant change in the profiles of concentration with distance along the particle bed.

As shown in Fig. 14, the initial velocity profiles approach the final velocity profiles in a nonmonotonic way and the difference between the initial and final particle profiles is significant, particularly within 100 particle diameters of the bed.

Figures 15 and 16 show profiles of particle vertical velocity and temperature. These profiles have nearly returned to zero and uniformity at a steady value for a particle bed after $10^6$ diameters of evolution.

Figure 17 indicates that the total particle flux has ceased to vary after this distance; while Fig. 18 focuses on the initial variation, which is significant over a distance of $10^4$ diameters. This is the variation that is accessible in laboratory wind tunnels [1,2,9,12,33,38,39].

## VI. CONCLUSIONS

We have outlined the development of a two-phase continuum theory for unsteady or nonuniform saltation that includes boundary conditions and stress relations for the particle phase. We have employed the MATLAB solver pdepe to solve the resulting system of equations for the uniform evolution in time that resulted from a small increase in the shear stress of the wind far from a particle bed. For these, the predictions of our model are similar to those of Sauermann *et al.* [6] who employ a simpler model, but differ from those of the Pahtz model [11,12] in at least one respect. For an arbitrary small change of the fluid shear stress, we obtain a nonmonotonic relaxation characterized by damped oscillations that are absent in the Pahtz model. Regarding the characteristic length scale of the relaxation process, our model suggests that the saturation length is proportional to $T/(\beta g) = (u_0^0)^2/(23\beta g) \approx 30(u_0^0)^2/g$, where $\beta$ is the coefficient in the linearized vertical flux. This result is analogous to those of the Sauermann *et al.* [6] and Pahtz models. It emphasizes that the relaxation process is crucially dependent of the splash process through the coefficient $\beta$.

We also treated nonuniform flows over a rigid base. We found, in particular, that for a given Shields number, the steady states for which the particle flux decreases with increasing particle holdup are unstable when permitted to spatially evolve, and they relax to the solution with the peak value of the particle flux. During the relaxation process, the particle holdup has to decrease to the value of the peak. Thus, the characteristic length scale of this process is expected to depend both on the deposition rate and the saltation hop length over a rigid bed. We find that for $S^* = 0.05$, the saturation length is about 100 times the saltation hop length, or about $10^7$ particle diameters.

Finally, we determined the steady, nonuniform solution for the flow over a particle bed that develops with distance from a steady solution over a rigid bed. The behavior of the particle flux in this transition has been successfully described by Sauermann *et al.* [6] in their two-equation continuum model. Our treatment involves boundary conditions that can distinguish between a rigid and a particle bed and a system of partial differential equations that predict profiles of concentration, particle, and wind velocity over the beds. This provides more information to test against measurements, in the context of a theory that employs fewer modeling parameters than that of Sauermann *et al.* [6]. We hope eventually to find a way to close the depth-averaged version of our equations and to better understand the relationship between the two models.

In any case, we believe that the development of the continuum theory outlined here should encourage additional measurements made in developing flows in wind tunnels (e.g., Refs. [1,2,9,12,33,38,39]) and tests of the modeling assumptions against the results of discrete simulations of saltation over rigid and particle beds [20–24]. We look forward to this activity.

## ACKNOWLEDGMENTS

The authors are grateful to the Max Planck Institute for Complex Systems, Dresden, Germany, where some of this work was carried out during the program geoflow16. J.T.J. acknowledges travel

support associated with his participation in the program received from US NSF Award No. 1619768 to Cornell University.

## APPENDIX

Here, we calculate the upward velocity

$$v_{\rm up} = \frac{N_0}{\xi_0}\frac{6}{\pi^2 T}\int_{\xi_0}^{\infty}\int_0^{\pi}(1-e^2)(\xi-\xi_0)\xi^2 e^{-\frac{1}{2T}[(\xi\cos\theta-u_0)^2+\xi^2\sin^2\theta]}\sin\theta d\theta d\xi, \tag{A1}$$

in which $1-e^2 = 1-A^2+2AB\sin\theta - B^2\sin^2\theta$.

The coefficient of $1-A^2$ is

$$\begin{aligned}
&\int_{\xi_0}^{\infty}\int_0^{\pi}(\xi-\xi_0)\xi^2 e^{-\frac{1}{2T}[(\xi\cos\theta-u_0)^2+\xi^2\sin^2\theta]}\sin\theta d\theta d\xi\\
&= \int_{\xi_0}^{\infty}(\xi-\xi_0)\xi^2 e^{-\frac{\xi^2+u_0^2}{2T}}\int_0^{\pi} e^{\frac{\xi u_0\cos\theta}{T}}\sin\theta d\theta d\xi\\
&= \frac{T}{u_0}\int_{\xi_0}^{\infty}(\xi-\xi_0)\xi e^{-\frac{\xi^2+u_0^2}{2T}}(e^{\frac{\xi u_0}{T}}-e^{-\frac{\xi u_0}{T}})d\xi\\
&= \frac{T}{u_0}\int_{\xi_0}^{\infty}(\xi-\xi_0)\xi\left[e^{-\frac{(\xi-u_0)^2}{2T}}-e^{-\frac{(\xi+u_0)^2}{2T}}\right]d\xi.
\end{aligned} \tag{A2}$$

Then,

$$\begin{aligned}
-\int_{\xi_0}^{\infty}(\xi-\xi_0)\xi e^{-\frac{(\xi+u_0)^2}{2T}}d\xi &= -\sqrt{2T}\int_{\frac{\xi_0+u_0}{\sqrt{2T}}}^{\infty}\left[2Tv_1^2-\sqrt{2T}(2u_0+\xi_0)v_1+u_0(u_0+\xi_0)\right]e^{-v_1^2}dv_1\\
&= -\sqrt{2T}\left[\frac{\xi_0+u_0}{\sqrt{2T}}T-\left(\frac{T}{2}\right)^{1/2}(2u_0+\xi_0)\right]e^{-\frac{(\xi_0+u_0)^2}{2T}}\\
&\quad -\left(\frac{\pi T}{2}\right)^{1/2}[T+u_0(u_0+\xi_0)]\mathrm{erfc}\left(\frac{\xi_0+u_0}{\sqrt{2T}}\right)
\end{aligned} \tag{A3}$$

and

$$\begin{aligned}
\int_{\xi_0}^{\infty}(\xi-\xi_0)\xi e^{-\frac{(\xi-u_0)^2}{2T}}d\xi &= \sqrt{2T}\int_{\frac{\xi_0-u_0}{\sqrt{2T}}}^{\infty}\left[2Tv_2^2+\sqrt{2T}(2u_0-\xi_0)v_2+u_0(u_0-\xi_0)\right]e^{-v_2^2}dv_2\\
&= \sqrt{2T}\left[\frac{\xi_0-u_0}{\sqrt{2T}}T+\left(\frac{T}{2}\right)^{1/2}(2u_0-\xi_0)\right]e^{-\frac{(\xi_0-u_0)^2}{2T}}\\
&\quad +\left(\frac{\pi T}{2}\right)^{1/2}[T+u_0(u_0-\xi_0)]\mathrm{erfc}\left(\frac{\xi_0-u_0}{\sqrt{2T}}\right).
\end{aligned} \tag{A4}$$

The coefficient of $2AB$ is

$$\int_{\xi_0}^{\infty}\int_0^{\pi}(\xi-\xi_0)\xi^2 e^{-\frac{1}{2T}[(\xi\cos\theta-u_0)^2+\xi^2\sin^2\theta]}\sin^2\theta d\theta d\xi = \int_{\xi_0}^{\infty}(\xi-\xi_0)\xi^2 e^{-\frac{\xi^2+u_0^2}{2T}}\int_0^{\pi} e^{\frac{\xi u_0\cos\theta}{T}}\sin^2\theta d\theta d\xi, \tag{A5}$$

with

$$\int_0^\pi e^{\frac{\xi u_0 \cos\theta}{T}} \sin^2\theta d\theta = \int_{-1}^1 e^{\frac{\xi u_0 v}{T}} (1-v^2)^{1/2} dv = \frac{T}{\xi u_0} \pi I_1\left(\frac{\xi u_0}{T}\right), \tag{A6}$$

$$\int_{\xi_0}^\infty \int_0^\pi (\xi - \xi_0)\xi^2 e^{-\frac{1}{2T}[(\xi\cos\theta - u_0)^2 + \xi^2 \sin^2\theta]} \sin^2\theta d\theta d\xi$$

$$= \pi \frac{T}{u_0} \int_{\xi_0}^\infty (\xi - \xi_0)\xi I_1\left(\frac{\xi u_0}{T}\right) e^{-\frac{\xi^2 + u_0^2}{2T}} d\xi$$

$$= \pi \frac{T^2}{4.6} e^{-\frac{(4.6)^2}{2}} \int_{x_0}^\infty (x - x_0) x I_1(4.6x) e^{-\frac{x^2}{2}} dx, \tag{A7}$$

where $x \equiv \xi/\sqrt{T}$, $x_0 \equiv \xi_0/\sqrt{T}$, and $4.6 = u_0/\sqrt{T}$.

With the approximation $I_1(4.6x)e^{-\frac{x^2}{2}} \doteq 3400 e^{-\frac{(x-4.6)^2}{2}}$,

$$\pi \frac{T^2}{4.6} e^{-\frac{(4.6)^2}{2}} \int_{x_0}^\infty (x - x_0) x I_1(4.6x) e^{-\frac{x^2}{2}} dx = 3400\pi \frac{T^2}{4.6} e^{-\frac{(4.6)^2}{2}} \int_{x_0}^\infty (x - x_0) x e^{-\frac{(x-4.6)^2}{2}} dx, \tag{A8}$$

where

$$\int_{x_0}^\infty (x - x_0) x e^{-\frac{(x-4.6)^2}{2}} dx$$

$$= \sqrt{2} \int_{\frac{x_0 - 4.6}{\sqrt{2}}}^\infty (\sqrt{2}v + 4.6 - x_0)(\sqrt{2}v + 4.6) e^{-v^2} dv$$

$$= \sqrt{2} \int_{\frac{x_0 - 4.6}{\sqrt{2}}}^\infty [2v^2 + \sqrt{2}(9.2 - x_0)v + 4.6(4.6 - x_0)] e^{-v^2} dv$$

$$= \sqrt{2} \left\{ \left[ \frac{\xi_0 - u_0}{\sqrt{2T}} + \frac{\sqrt{2}}{2}(9.2 - x_0) \right] e^{-\frac{(\xi_0 - u_0)^2}{2T}} + \frac{1}{2}[1 + 4.6(4.6 - x_0)]\sqrt{\pi} \operatorname{erfc}\left(\frac{\xi_0 - u_0}{\sqrt{2T}}\right) \right\}. \tag{A9}$$

The coefficient of $-B^2$ is

$$\int_{\xi_0}^\infty (\xi - \xi_0)\xi^2 e^{-\frac{\xi^2 + u_0^2}{2T}} \int_0^\pi e^{\frac{\xi u_0 \cos\theta}{T}} \sin^3\theta d\theta d\xi, \tag{A10}$$

with

$$\int_0^\pi e^{\frac{\xi u_0 \cos\theta}{T}} \sin^3\theta d\theta = \int_{-1}^1 e^{\frac{\xi u_0 v}{T}} (1 - v^2) dv = 4\left(\frac{T}{\xi u_0}\right)^3 \left[ \frac{\xi u_0}{T} \cosh\left(\frac{\xi u_0}{T}\right) - \sinh\left(\frac{\xi u_0}{T}\right) \right], \tag{A11}$$

$$\int_{\xi_0}^\infty (\xi - \xi_0)\xi^2 e^{-\frac{\xi^2 + u_0^2}{2T}} \int_0^\pi e^{\frac{\xi u_0 \cos\theta}{T}} \sin^3\theta d\theta d\xi$$

$$= 4\left(\frac{T}{u_0}\right)^3 \int_{\xi_0}^\infty \frac{(\xi - \xi_0)}{\xi} \left[ \frac{\xi u_0}{T} \cosh\left(\frac{\xi u_0}{T}\right) - \sinh\left(\frac{\xi u_0}{T}\right) \right] e^{-\frac{\xi^2 + u_0^2}{2T}} d\xi$$

$$= 2\left(\frac{T}{u_0}\right)^3 \int_{\xi_0}^\infty (\xi - \xi_0) \left[ \frac{u_0}{T} \left( e^{-\frac{(u_0 - \xi)^2}{2T}} + e^{-\frac{(u_0 + \xi)^2}{2T}} \right) - \frac{1}{\xi} \left( e^{-\frac{(u_0 + \xi)^2}{2T}} - e^{-\frac{(u_0 - \xi)^2}{2T}} \right) \right] d\xi. \tag{A12}$$

Then,

$$\int_{\xi_0}^{\infty}(\xi-\xi_0)\left(\frac{u_0}{T}-\frac{1}{\xi}\right)e^{-\frac{(\xi+u_0)^2}{2T}}d\xi$$
$$=\sqrt{2T}\int_{\frac{\xi_0+u_0}{\sqrt{2T}}}^{\infty}[\sqrt{2T}v_1-(\xi_0+u_0)]\left(\frac{u_0}{T}-\frac{1}{\sqrt{2T}v_1-u_0}\right)e^{-v_1^2}dv_1$$
$$=\sqrt{2T}\int_{\frac{\xi_0+u_0}{\sqrt{2T}}}^{\infty}\left[\sqrt{2T}\frac{u_0}{T}v_1-1-(\xi_0+u_0)\frac{u_0}{T}+\frac{\xi_0/\sqrt{2T}}{v_1-u_0/\sqrt{2T}}\right]e^{-v_1^2}dv_1, \tag{A13}$$

in which

$$\int_{\frac{\xi_0+u_0}{\sqrt{2T}}}^{\infty}\frac{\xi_0/\sqrt{2T}}{v_1-u_0/\sqrt{2T}}e^{-v_1^2}dv_1=\frac{\xi_0}{\sqrt{2T}}\int_1^{\infty}\frac{1}{w}e^{-\frac{(\xi_0 w+u_0)^2}{2T}}dw\doteq\frac{\xi_0}{\sqrt{2T}}\int_1^{\infty}e^{-\frac{(\xi_0 w+u_0)^2}{2T}}dw$$
$$=\frac{\xi_0}{\sqrt{2T}}\int_{\frac{\xi_0+u_0}{\sqrt{2T}}}^{\infty}e^{-v^2}dv=\frac{\xi_0}{\sqrt{2T}}\frac{\sqrt{\pi}}{2}\mathrm{erfc}\left(\frac{\xi_0+u_0}{\sqrt{2T}}\right) \tag{A14}$$

and

$$\int_{\frac{\xi_0+u_0}{\sqrt{2T}}}^{\infty}\left[\sqrt{2T}\frac{u_0}{T}v_1+1-(\xi_0+u_0)\frac{u_0}{T}\right]e^{-v_1^2}dv_1$$
$$=\left(\frac{T}{2}\right)^{1/2}\frac{u_0}{T}e^{-\frac{(\xi_0+u_0)^2}{2T}}+\left[1-(\xi_0+u_0)\frac{u_0}{T}\right]\frac{\sqrt{\pi}}{2}\mathrm{erfc}\left(\frac{\xi_0+u_0}{\sqrt{2T}}\right). \tag{A15}$$

Similarly,

$$\int_{\xi_0}^{\infty}(\xi-\xi_0)\left(\frac{u_0}{T}-\frac{1}{\xi}\right)e^{-\frac{(\xi-u_0)^2}{2T}}d\xi$$
$$=\sqrt{2T}\int_{\frac{\xi_0-u_0}{\sqrt{2T}}}^{\infty}[\sqrt{2T}v_2-(\xi_0-u_0)]\left(\frac{u_0}{T}-\frac{1}{\sqrt{2T}v_2+u_0}\right)e^{-v_2^2}dv_2$$
$$=\sqrt{2T}\int_{\frac{\xi_0-u_0}{\sqrt{2T}}}^{\infty}\left[\sqrt{2T}\frac{u_0}{T}v_2+1-(\xi_0-u_0)\frac{u_0}{T}-\frac{\xi_0/\sqrt{2T}}{v_2+u_0/\sqrt{2T}}\right]e^{-v_2^2}dv_2, \tag{A16}$$

in which

$$-\int_{\frac{\xi_0-u_0}{\sqrt{2T}}}^{\infty}\frac{1}{v_2+u_0/\sqrt{2T}}e^{-v_2^2}dv_2=-\int_{\xi_0/\sqrt{2T}}^{\infty}\frac{1}{w}e^{-(w-u_0/\sqrt{2T})^2}dw\doteq-0.32\int_{\frac{\xi_0-u_0}{\sqrt{2T}}}^{\infty}e^{-v^2}dv$$
$$=-0.32\frac{\sqrt{\pi}}{2}\mathrm{erfc}\left(\frac{\xi_0-u_0}{\sqrt{2T}}\right) \tag{A17}$$

and

$$\int_{\frac{\xi_0-u_0}{\sqrt{2T}}}^{\infty}\left[\sqrt{2T}\frac{u_0}{T}v_2+1-(\xi_0-u_0)\frac{u_0}{T}\right]e^{-v_2^2}dv_2$$
$$=\left(\frac{T}{2}\right)^{1/2}\frac{u_0}{T}e^{-\frac{(\xi_0-u_0)^2}{2T}}+\left[1-(\xi_0-u_0)\frac{u_0}{T}\right]\frac{\sqrt{\pi}}{2}\mathrm{erfc}\left(\frac{\xi_0-u_0}{\sqrt{2T}}\right). \tag{A18}$$

Upon collecting only those terms with an argument $(\xi_0 - u_0)/\sqrt{2T}$,

$$v_{\rm up} = \frac{N_0}{\xi_0}\frac{6}{\pi^2 T}(1-A^2)\frac{T^{5/2}}{u_0}\left\{\frac{u_0}{\sqrt{T}}e^{-\frac{(\xi_0-u_0)^2}{2T}} + \left(\frac{\pi}{2}\right)^{1/2}\left[1+\frac{u_0(u_0-\xi_0)}{T}\right]\mathrm{erfc}\left(\frac{\xi_0-u_0}{\sqrt{2T}}\right)\right\}$$
$$+ 2AB(3400)\pi\frac{T^{5/2}}{u_0}\mathrm{e}^{-\frac{u_0^2}{2}}\left\{\frac{u_0}{\sqrt{T}}e^{-\frac{(\xi_0-u_0)^2}{2T}} + \left(\frac{\pi}{2}\right)^{1/2}\left[1+\frac{u_0(u_0-\xi_0)}{T}\right]\mathrm{erfc}\left(\frac{\xi_0-u_0}{\sqrt{2T}}\right)\right\}$$
$$- B^2 2\frac{T^{5/3}}{u_0}\frac{T}{u_0^2}\left\{\frac{u_0}{\sqrt{T}}e^{-\frac{(\xi_0-u_0)^2}{2T}} + \left(\frac{\pi}{2}\right)^{1/2}\left[1+\frac{u_0(u_0-\xi_0)}{T}-0.32\right]\mathrm{erfc}\left(\frac{\xi_0-u_0}{\sqrt{2T}}\right)\right\}, \tag{A19}$$

or

$$v_{\rm up} = \frac{N_0}{\xi_0}\frac{6}{\pi^2}\frac{T^{3/2}}{u_0}\left[\left(1-A^2+6800\pi AB e^{-\frac{u_0^2}{2T}} - 2B^2\frac{T}{u_0^2}\right)\right.$$
$$\times\left\{\frac{u_0}{\sqrt{T}}e^{-\frac{(\xi_0-u_0)^2}{2T}} + \left(\frac{\pi}{2}\right)^{1/2}\left[1-\frac{u_0(\xi_0-u_0)}{T}\right]\mathrm{erfc}\left(\frac{\xi_0-u_0}{\sqrt{2T}}\right)\right\}$$
$$\left.+ 2(0.32)B^2\frac{T}{u_0^2}\left(\frac{\pi}{2}\right)^{1/2}\mathrm{erfc}\left(\frac{\xi_0-u_0}{\sqrt{2T}}\right)\right]. \tag{A20}$$

Expressing this as a function of $u_0$, using $T = (u_0/4.6)^2$,

$$v_{\rm up} = \frac{N_0}{\xi_0}\frac{6}{\pi^2}\frac{T^{3/2}}{u_0}\left[\left(1-A^2+6800\pi AB e^{-\frac{u_0^2}{2T}} - 2B^2\frac{T}{u_0^2}\right)\right.$$
$$\times\left\{\frac{u_0}{\sqrt{T}}e^{-\frac{(\xi_0-u_0)^2}{2T}} + \left(\frac{\pi}{2}\right)^{1/2}\left[1-\frac{u_0(\xi_0-u_0)}{T}\right]\mathrm{erfc}\left(\frac{\xi_0-u_0}{\sqrt{2T}}\right)\right\}$$
$$\left.+ 0.64\left(\frac{\pi}{2}\right)^{1/2}B^2\frac{T}{u_0^2}\mathrm{erfc}\left(\frac{\xi_0-u_0}{\sqrt{2T}}\right)\right]. \tag{A21}$$

Finally, with $A = 0.87$ and $B = 0.72$,

$$v_{\rm up} = 0.002u_0^2\left[\left[0.53\left\{4.6e^{-\frac{(4.6)^2(40-u_0)^2}{2u_0^2}} + \left(\frac{\pi}{2}\right)^{1/2}\left[1-\frac{(4.6)^2(40-u_0)}{u_0}\right]\mathrm{erfc}\left(4.6\frac{40-u_0}{\sqrt{2}u_0}\right)\right\}\right.\right.$$
$$\left.\left.+\ 0.02\,\mathrm{erfc}\left(4.6\frac{40-u_0}{\sqrt{2}u_0}\right)\right]\right]. \tag{A22}$$


[1] R. A. Bagnold, The transport of sand by wind, Geograph. J. **89**, 409 (1937).

[2] R. A. Bagnold, *The Physics of Blown Sand and Desert Dunes* (Methuen, New York, 1941).

[3] M. P. Almeida, J. S. Andrade, and H. J. Herrmann, Aeolian transport of sand, Eur. Phys. J. E **22**, 195 (2007).

[4] J. F. Kok, E. J. R. Parteli, T. I. Michaels, and D. B. Karam, The physics of wind-blown sand and dust, Rep. Prog. Phys. **75**, 106901 (2012).

[5] E. J. R. Parteli, K. Kroy, H. Tsoar, J. S. Andrade, T. Pöschel, and H. J. Herrmann, Morphodynamic modeling of aeolian dunes: Review and future plans, Eur. Phys. J. Spec. Top. **223**, 2269 (2014).

[6] G. Sauermann, K. Kroy, and H. J. Herrmann, A continuum saltation model for sand dunes, Phys. Rev. E **64**, 031305 (2001).

[7] P. Hersen, S. Douady, and B. Andreotti, Relevant Length Scale for Barchan Dunes, Phys. Rev. Lett. **89**, 264301 (2002).
[8] P. Claudin and B. Andreotti, A scaling law for aeolian dunes on Mars, Venus, Earth, and for subaqueous ripples, Earth Planet. Sci Lett. **252**, 30 (2006).
[9] B. Andreotti, P. Claudin, and O. Pouliquen, Measurements of the aeolian sand transport saturation length, Geomorph **123**, 343 (2010).
[10] T. Pähtz, J. F. Kok, E. J. R. Parteli, and H. J. Herrmann, Flux Saturation Length of Sediment Transport, Phys. Rev. Lett. **111**, 218002 (2013).
[11] T. Pähtz, E. J. R. Parteli, J. F. Kok, and H. J. Herrmann, Analytical model for flux saturation in sediment transport, Phys. Rev. E **89**, 052213 (2014).
[12] M. Creyssels, P. Dupont, A. O. el Moctar, A. Valance, I. Cantat, J. T. Jenkins, J. M. Pasini, and K. R. Rasmussen, Saltating particles in a turbulent boundary layer: Experiment and theory, J. Fluid Mech. **625**, 47 (2009).
[13] J. T. Jenkins, I. Cantat, and A. Valance, Continuum model for steady, fully developed saltation above a horizontal particle bed, Phys. Rev. E **82**, 020301 (2010).
[14] T.-J. Hsu, J. T. Jenkins, and P. P.-L. Liu, On two-phase sediment transport: Dilute flow, J. Geophys. Res.: Oceans **108**, 3057 (2003).
[15] J. M. Pasini and J. T. Jenkins, Aeolian transport with collisional suspension, Philos. Trans. R. Soc. London **363**, 1625 (2005).
[16] M. V. Carneiro, N. A. M. Aráujo, T. Pähtz, and H. J. Herrmann, Midair Collisions Enhance Saltation, Phys. Rev. Lett. **111**, 058001 (2013).
[17] D. Beladjine, M. Ammi, L. Oger, and A. Valance, Collision process between an incident bead and a three-dimensional granular packing, Phys. Rev. E **75**, 061305 (2007).
[18] L. Oger, M. Ammi, A. Valance, and D. Beladjine, Discrete element method studies of the collision of one rapid sphere on 2D and 3D packings, Eur. Phys. J. E **17**, 467 (2005).
[19] J. Crassous, D. Beladjine and A. Valance, Impact of a Projectile on a Granular Medium Described by a Collision Model, Phys. Rev. Lett. **99**, 248001 (2007).
[20] O. Durán, P. Claudin, and B. Andreotti, On aeolian transport: Grain-scale interactions, dynamical mechanisms and scaling laws, Aeolian Res. **3**, 243 (2011).
[21] O. Durán, B. Andreotti, and P. Claudin, Numerical simulation of turbulent sediment transport, from bed load to saltation, Phys. Fluids **24**, 103306 (2012).
[22] O. Durán, P. Claudin, and B. Andreotti, Direct numerical simulations of aeolian sand ripples, Proc. Natl. Acad. Sci. USA **111**, 15665 (2014).
[23] O. Durán, B. Andreotti, and P. Claudin, Turbulent and viscous sediment transport a numerical study, Adv. Geosci. **37**, 73 (2014).
[24] T. Pähtz, A. Omeradžić, M. V. Carneiro, N. A. M Araújo, and H. J. Herrmann, Discrete element method simulations of the saturation of aeolian sand transport, Geophys. Res. Lett. **42**, 2063 (2015).
[25] A. Fourrière, P. Claudin, and B. Andreotti, Bedforms in a turbulent stream: Formation of ripples by primary linear instability and of dunes by nonlinear pattern coarsening, J. Fluid Mech. **649**, 287 (2010).
[26] E. J. R. Parteli, J. S. Andrade, and H. J. Herrmann, Transverse Instability of Dunes, Phys. Rev. Lett. **107**, 188001 (2011).
[27] F. Charru, B. Andreotti, and P. Claudin, Sand ripples and dunes, Annu. Rev. Fluid Mech. **45**469 (2013).
[28] P. S. Jackson and J. C. R. Hunt, Turbulent wind flow over a low hill, Q. J. R. Meteorol. Soc. **101**, 929 (1975).
[29] J. C. R. Hunt, S. Leibovich, and K. J. Richards, Turbulent shear flows over low hills, Q. J. R. Meteorol. Soc. **114**, 1435 (1988).
[30] W. S. Weng, D. J. Carruthers, J. C. R. Hunt, A. Warren, G. F. S. Wiggs, and I. Livingstone, Air flow and sand transport over sand dunes, in *Aeolian Grain Transport*, edited by O. E. Barndorff-Nielson and B. B. Willetts, Acta Mechanica Supplement Vol. 2 (Springer, Vienna, 1991), pp. 1–22.
[31] K. Kroy, G. Sauermann, and H. J. Herrmann, Minimal model for aeolian sand dunes, Phys. Rev. E **66**, 031302 (2002).

[32] K. Kroy, G. Sauermann, and H. J. Herrmann, A Minimal Model for Sand Dunes, Phys. Rev. Lett. **88**, 054301 (2002).
[33] T.-D. Ho, A. Valance, P. Dupont, and A. Ould El Moctar, Aeolian sand transport: Length and height distributions of saltation trajectories, Aeolian Res. **12**, 65 (2014).
[34] J. T. Jenkins and A. Valance, Periodic trajectories in aeolian sand transport, Phys. Fluids **26**, 073301 (2014).
[35] E. R. Van Driest, On turbulent flow near a wall, J. Aeronaut. Sci. **23**, 1007 (1956).
[36] R. S. Anderson and P. K. Haff, Wind modification and bed response during saltation of sand in air, in *Aeolian Grain Transport* (Ref. [30]), pp. 21–51.
[37] D. Berzi, J. T. Jenkins, and A. Valance, Periodic saltation over hydrodynamically rough beds: Aeolian to aquatic, J. Fluid Mech. **786**, 10 (2016).
[38] T.-D. Ho, A. Valance, P. Dupont, and A. Ould El Moctar, Scaling Laws in Aeolian Sand Transport, Phys. Rev. Lett. **106**, 094501 (2011).
[39] T.-D. Ho, Etude expérimentale du transport de particules dans une couche limite turbulente, Doctoral thesis, Université de Rennes, 2012.